DOI 10.1002/pssa.201532325

Synthesis of vanadium oxide films with controlled morphologies: Impact on the metal–insulator transition behaviour

Sunil Kumar*,[1], Damien Lenoble[1], Francis Maury[2], and Naoufal Bahlawane,[1]**

[1] Luxembourg Institute of Science and Technology (LIST), 5, avenue des Hauts-Fourneaux, 4362 Esch sur Alzette, Luxembourg
[2] CIRIMAT, ENSIACET-4, allee E. Monso, 31432 Toulouse, France

Keywords chemical vapour deposition, morphology, thin films, vanadium oxide

* Corresponding author: e-mail sunilkumar.channam@list.lu, Phone: +352 661 128 362, Fax: +352 275 885
** e-mail naoufal.bahlawane@list.lu

Precise control over the growth of VO_2 films with different morphologies is achieved by varying the deposition parameters in the DLI-MOCVD process such as temperature, pressure, concentration of precursor and time of deposition. In this study, thin films of VO_2 with wide range of morphologies having Metal to Insulator Transition (MIT) temperature of (τ_c) $\sim$ 52 °C were deposited. Adjusting the process parameters has allowed the growth of highly porous nanocrystalline films and dense microcrystalline films with controlled crystallite size up to several hundred nanometres. Vanadium (V) oxy tri-isopropoxide was used in this study as a single source precursor. Porous films lead to a diffuse change in resistivity across the transition temperature while the crystalline films have sharp and high resistivity drop ($\Delta\rho$). This enabled a qualitative study of the MIT behaviour with respect to the microstructure of the films and correlates the effect of deposition conditions to the obtained morphologies. Fine control over the morphology without additional doping or post deposition process provides the ability to tailor VO_2 thin films for their respective applications. Scanning electron microscopy, Raman spectroscopy and X-ray diffraction were used to characterize the microstructure of the films while electrical resistivity measurements were carried out to observe the MIT behaviour of the films.

1 Introduction Vanadium (IV) oxide (VO_2) undergoes a reversible phase transition from an insulating monoclinic to a conducting rutile structure around the transition temperature (τ_c) 68–70 °C [1]. Intrinsic material properties like electrical resistivity, optical transmission and mechanical strain undergo abrupt changes occurring at MIT [2]. This remarkable behaviour of the material has sparked immense interest and has been actively researched for potential applications ranging from ultra-fast nano-electronic switches, transistors, thermoelectric devices and thermochromic smart windows [3–6].

In most cases, however, the focus is always mainly on reducing the τ_c closer to room temperature. Doping with impurities is one way to reduce the τ_c but resulted in sacrificing the sharpness of the phase transition [7–10]. Thin undoped nanocrystalline VO_2 films were reported exhibiting the MIT at τ_c as low as 55 °C. The growth of single phase VO_2 remains a challenge due to the fact that a number of stable phases of vanadium oxides could form in a narrow range of composition, thus, requiring a strict control on growth conditions for obtaining a single pure phase of VO_2 [11]. Various types of thin film deposition techniques have been employed for VO_2 film synthesis like pulsed laser deposition (PLD) [5, 12], molecular beam epitaxy (MBE) [3], magnetron sputtering [13], chemical vapour deposition (CVD) [14–17], sol–gel processing [18, 19] and atomic layer deposition [20–22]. In this study, we use direct liquid injection–metal organic chemical vapour deposition (DLI–MOCVD) and a single source precursor to grow VO_2 films of varying thickness and microstructure.

Several authors have reported results correlating the film thickness, grain size and crystallinity with the MIT [23–26] and provided rather conflicting views relating film morphology and MIT behaviour as each case has only one or limited types of morphologies being studied.

Therefore, it is important to properly understand this property with respect to various microstructures and their influence on the grain boundary density and crystallinity. In this study, we grow single phase VO_2 films of various morphologies and crystallinities by varying the deposition parameters to compare the MIT behaviour, hysteresis width (ΔT) and $\Delta\rho$ corresponding to each unique microstructure.

2 Experimental

2.1 Deposition of VO_2 Thin films of VO_2 were deposited on silicon substrates by DLI–MOCVD in a warm wall vertical stagnation point flow reactor. Low concentration (5×10^{-3} M) ethanol solutions of 99.9% pure V oxy-tri-isopropoxide ($[VO(O^iPr)_3]$ were used as the precursor. Liquid injection was performed in an evaporation tube maintained at 200 °C to secure an instantaneous vapourization of the precursor solution. Substrates were maintained at a constant temperature within the 400–600 °C range during deposition. The precursor injection was maintained at 4 Hz with 2 ms opening time resulting in a liquid flow rate of 2.5 ml min^{-1}. Nitrogen was used as the carrier gas with a flow rate, 40 sccm and the chamber pressure being adjusted in the 3–9 mbar range.

Time of deposition was adjusted from 15 to 180 min allowing the growth of different film thicknesses. Substrates were allowed to cool to room temperature in nitrogen atmosphere under vacuum before withdrawing from the chamber and no post deposition annealing was performed. All the samples were handled in air after deposition.

2.2 Characterization Film thickness was measured using an Alpha step d-500 Profilometer from KLA-Tencor and FEI Helios Nanolab 650^{TM} scanning electron microscope (SEM). Surface and cross-sectional morphologies were characterized by SEM at a working distance of 4 mm with 25 kV voltage.

X-ray diffraction (XRD) was used to characterize the films using the Bruker D8, with CuK_α as the X-ray source. Data were collected in the θ–2θ (locked couple) mode from 2θ of 20 to 60° with a step size of 0.05°.

Raman spectroscopy was performed using an InVia Raman spectrometer from Renishaw with a 532 nm laser at low power of 0.2 mW to avoid non-controlled surface heating and the resulting phase transition upon laser irradiation. The resistivity of the films was measured using a Hall effect measurement system HMS-3000 in van der Pauw configuration. Temperature-dependent resistivity measurements were performed by placing the sample on a heating stage, while a thermocouple was placed on the sample to measure the surface temperature.

The characterization techniques employed in this study provide complementary insights to understand the interplay between the growth control parameters, film characteristics and the corresponding MIT behaviour.

3 Results and discussion CVD enables a convenient number of parameters of deposition namely (i) temperature of deposition, (ii) chamber pressure, (iii) concentration of the precursor and (iv) time of deposition. The main objective of this study is to obtain different morphologies of VO_2 by varying the growth parameters and to investigate their impact on MIT behaviour.

3.1 Deposition temperature An increase in grain size and crystalline morphology is observed when the temperature of deposition was increased from 450 to 600 °C. Figure 1 shows SEM micrographs of films deposited at various temperatures. It depicts a transition of morphology from a porous nanocrystalline to a compact microcrystalline to well-formed large crystallites of VO_2. Thickness of the resulting films was measured at 1.4 μm, 800 and 200 nm for the deposition temperatures of 450, 500 and 600 °C, respectively.

X-ray diffractograms and Raman spectra, shown in Fig. 2, reveal single phase growth of monoclinic VO_2 in this temperature range, Raman vibrational peaks observed at 141,192, 222, 310, 387, 496 and 613 all correspond to Ag mode VO_2. No significant change was observed in the Raman spectra when the deposition temperature was increased from 450 to 600 °C.

3.2 Precursor concentration Film thickness and microstructure depend on precursor concentration for MOCVD process, a 2.5 and 5 mM of V oxy tri-isopropoxide in absolute ethanol solution was used as the precursor.

At 500 °C, VO_2 films with high porosity and thickness of 2.2 μm were grown with a 5 mM concentrated precursor solution which contrasts the films grown at 2.5 mM featuring a smooth surface comprising individual large crystallites of VO_2 of thickness 190 nm forming across the surface as shown in Fig. 3.

3.3 Deposition time Highly crystalline well-ordered VO_2 films were grown with 2.5 mM precursor

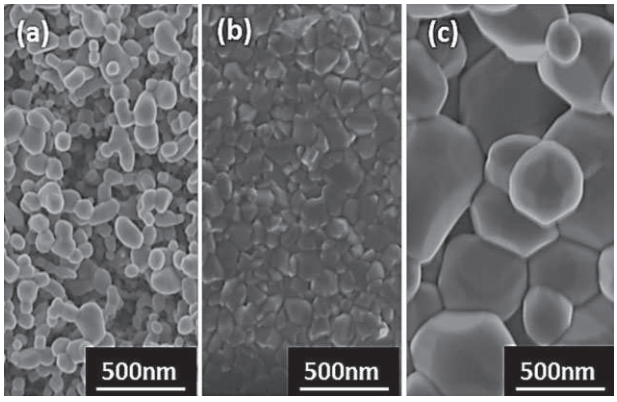

Figure 1 SEM micrographs of VO_2 films (a), (b) and (c) deposited at 450, 500 and 600 °C, respectively (chamber pressure 6 mbar). The average grain size is (a) 14.8, (b) 15 and (c) 130 nm.

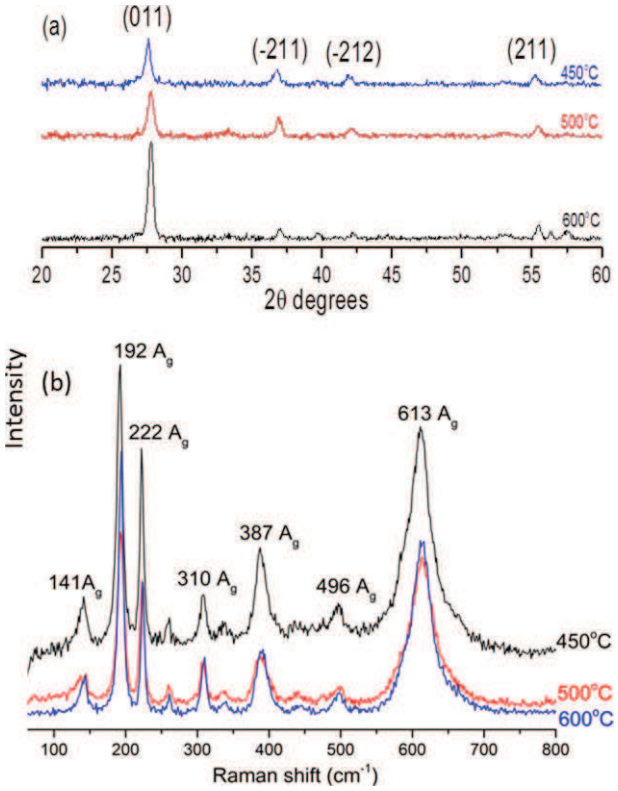

Figure 2 X-ray diffraction (a) and Raman spectra (b) of films deposited at 450, 500 and 600 °C, respectively. The peaks indicated for XRD correspond to PDF data card no. 00-009-0142 [8, 24, 27] and Raman peaks observed also indicate the formation of monoclinic VO_2 [27–31].

concentration. Shown in Fig. 4 are cross-section SEM micrographs of films deposited at 575 °C for 15, 30 and 120 min, revealing film thicknesses of 90, 150 and 720 nm, respectively. The film thickness at different times corresponds to a constant growth rate $(5.6 \pm 0.6)\,\mathrm{nm\,min^{-1}}$ without an incubation time.

The crystals grew anisotropically while retaining the single layer morphology. Hence, the increase in the film thickness is due to the growth and the merging of individual grains rather than a formation of multi-layered film composed of several microcrystalline grains. This structure reveals the high surface diffusion of the deposition species.

3.4 Chamber pressure With increasing chamber pressure, the films exhibit an increase in the surface roughness as shown in Fig. 5. The two-dimensional morphology at low pressure is partially replaced by a three-dimensional flaky sheet. Although cross-section inspection shows that early stage of deposition yields a similar morphology in the 3–9 mbar pressure range.

It is evident from Fig. 5e and f that formation of these flakes is favoured at higher chamber pressures, while simultaneously resulting in films with increased porosity and surface roughness. On close inspection of the flakes shown in Fig. 6, it was revealed that they are in fact formed

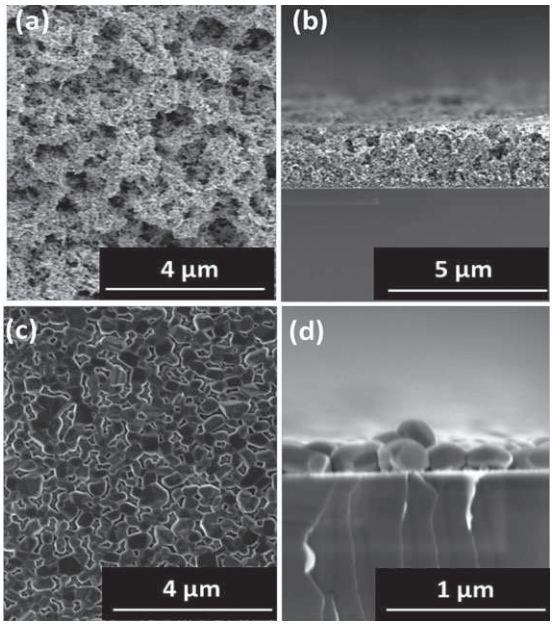

Figure 3 (a, c) Surface and (b, d) cross-section SEM micrographs of VO_2 films grown at 500 °C with 5 (a, b) and 2.5 mM (c, d) precursor concentration at total pressure 9 mbar.

by the aggregation of nanocrystalline grains of VO_2 similar to the film shown in Fig. 1a. These small nanocrystalline grains grew upwards at higher pressure and form a microstructure similar to petals in a rose flower. This type of morphology can be very well suited to gas sensing or absorbing applications where high porosity combined with high and accessible surface area play a key role in determining the effectiveness of the device.

3.5 MIT behaviour of different morphologies It is important to note that due to seemingly numerous ways of synthesising VO_2 films exhibiting MIT behaviour and equally varied number if not more ways of measuring this transition, a wide variety of measurement procedures have been reported like resistivity, transmittance, Raman spectra

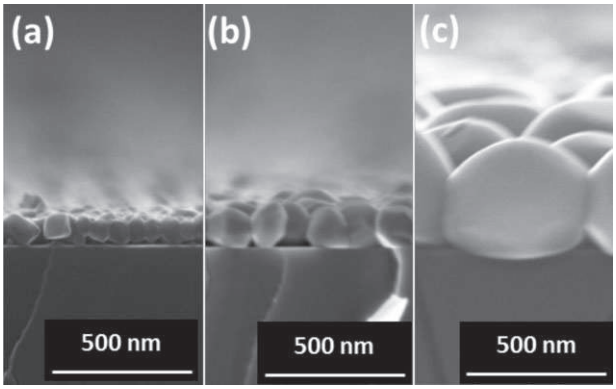

Figure 4 SEM cross-section micrographs of VO_2 films deposited at 575 °C for the duration of (a) 15, (b) 30 and (c) 120 min.

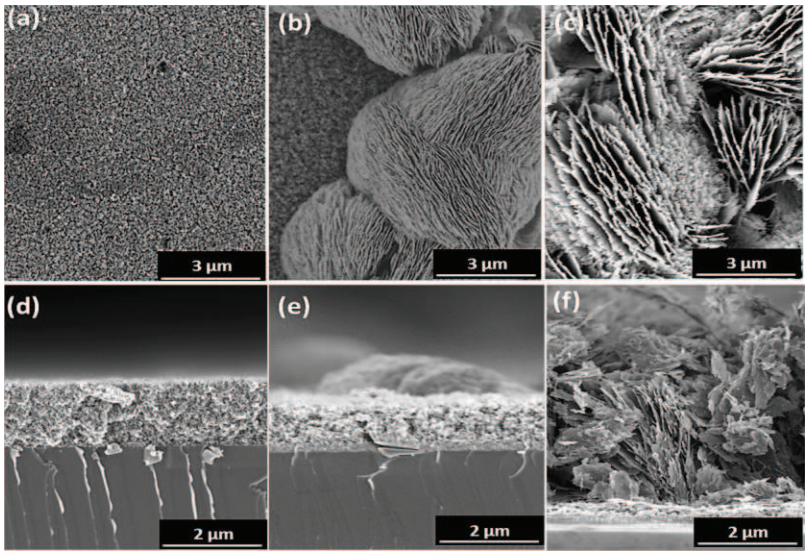

Figure 5 (a) (b) (c) SEM surface micrographs and (d) (e) (f) are the cross-section of VO_2 films deposited at chamber pressure 3, 6 and 9 mbar, respectively (temperature 450 °C, concentration 2.5 mM).

across the τ_c. To be able to compare the ΔT and τ_c for different morphologies, we chose a simple four-point probe resistivity measurement system, which sounds as the most prevalent method depicting the quality of films while still obtaining enough information about the films characteristics.

Electrical resistivity of the films was measured during heating and cooling of the sample in the 20–90 °C temperature window. This offers a convenient way to measure ΔT which does not extend beyond this temperature interval.

It is widely reported that τ_c of VO_2 bulk crystals is between 68–72 °C [1] with the ratio of resistivity in insulating (monoclinic) phase to the metallic (rutile) phase of the order of 10^5. Epitaxial films were reported to exhibit similar properties seen in single-bulk crystals [12, 32]. Whereas polycrystalline films have the tendency to have a smaller-resistivity drop and broader-hysteresis curve [5, 33, 34].

The top and bottom hysteresis plots shown in Fig. 7 correspond to the films depicted in Fig. 4a and b, respectively, which have similar morphology. The films are composed of a single layer of well-formed grains. VO_2 film in Fig. 4a resembles an epitaxial film in appearance with all grains having the same size and shape resulting in higher resistivity drop ($\Delta\rho$) and a narrow ΔT of 7 °C. While the film in Fig. 4b has a larger grain size but lack uniform size distribution as observed in thinner films, resulting in a broader ΔT of 12 °C. Films with higher density of grain boundaries and smaller grain size exhibit a diffuse MIT behaviour with a broad ΔT. The τ_c for both film morphologies is same at ~52 °C in the heating phase. In Fig. 8, the top and bottom hysteresis curves correspond to

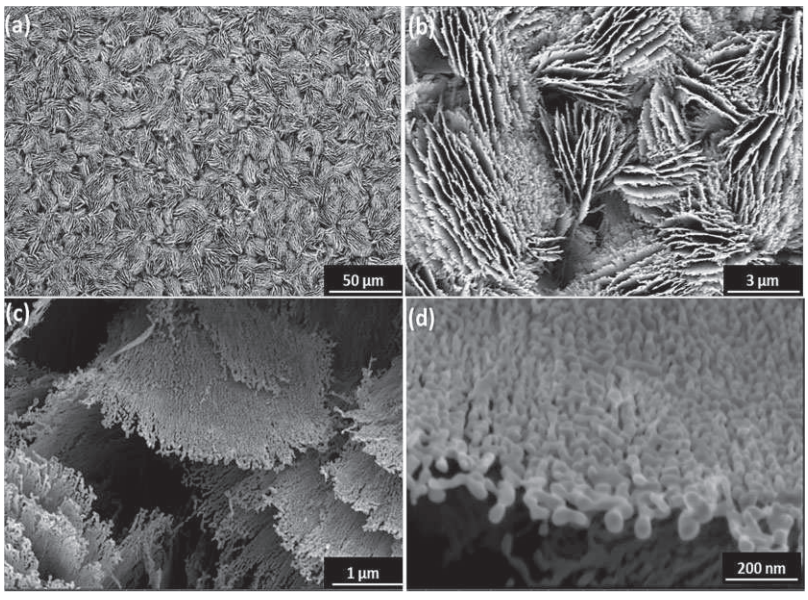

Figure 6 Surface micrographs of VO_2 film grown at 9 mbar shown at different magnifications (temperature 450 °C, concentration 2.5 mM). The average grain size is ~16.45 nm.

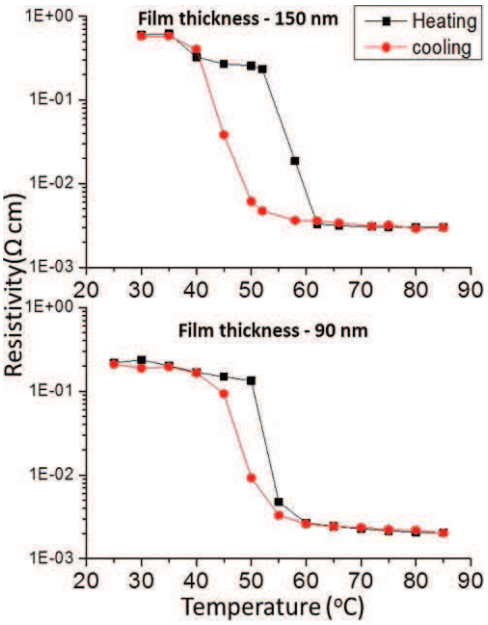

Figure 7 Comparison of the MIT behaviour of VO_2 film of thickness 150 and 90 nm for the top and bottom plot, respectively.

the morphologies as shown in Fig. 1a (porous) and b (compact), respectively.

Due to the smaller grain size and the porosity of the film in Fig. 1a, $\Delta\rho$ is diminished and the ΔT is broadened. Films with a compact microstructure, as shown in Fig. 1b, exhibit a narrower ΔT and sharper $\Delta\rho$ compared to a porous film. It is, however, interesting to note that the MIT temperature remains relatively unchanged at $\sim$52 °C during the heating

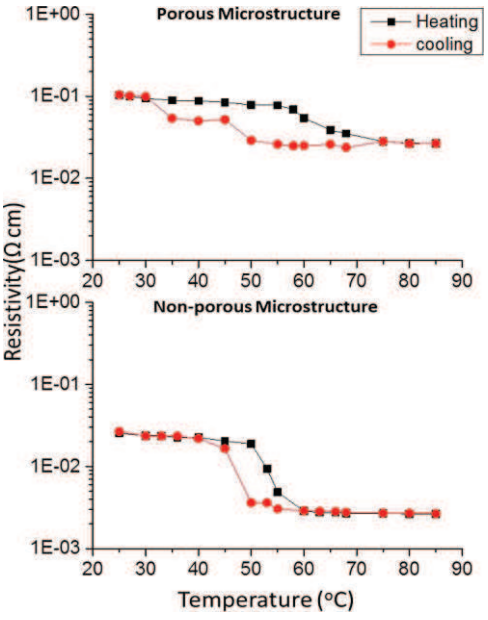

Figure 8 Comparison of the MIT behaviour of VO_2 with porous (top) and compact (bottom) films with the thickness of 1.4 μm each.

phase irrespective of the microstructure. On comparing the hysteresis curves obtained from the morphologies of Figs. 4a and 1b shown as the bottom curves of Figs. 7 and 8; we observe a higher $\Delta\rho$ and lower ΔT for films with better crystallinity.

4 Conclusions Thin films of VO_2 with different microstructures and morphologies were grown by MOCVD starting from $[VO(O^iPr)_3]$. This process was used to grow films of thickness ranging from 90 nm to 3 μm with fine control over porosity, crystallinity and grain size. This study reveals that morphology of VO_2 plays a pivotal role on the MIT behaviour. Film thickness, grain size, porosity, crystallinity and shape of the crystallites all have an impact on the ΔT, $\Delta\rho$ and τ_c. Having achieved a precise control over the growth of the films and the resulting microstructure, we have the freedom and ability to fine tune the film growth and MIT as per the desired application.

Acknowledgement The authors would like to acknowledge Luxembourg Institute of Science and technology (LIST) for providing the financial support for this work conducted at its Materials Research and Technology Laboratory.

References

[1] F. J. Morin, Phys. Rev. Lett. **3**(1), 34–36 (1959).
[2] J. Nag and R. Jr, J. Phys.: Condens. Matter **20**, 264016 (2008).
[3] Z. Yang, C. Ko, and S. Ramanathan, Annu. Rev. Mater. Res. **41**, 337–367 (2011).
[4] A. L. Pergament, G. B. Stefanovich, and A. A. Velichko, J. Sel. Top. Nanoelectron. Comput. 24–43 (2013).
[5] M. Warwick and R. Binions, J. Mater. Chem. A **2**, 3275–3292 (2013).
[6] M. A. Kats, R. Blanchard, S. Zhang, P. Genevet, C. Ko, S. Ramanathan, and F. Capasso, Phys. Rev. X **3**(4), 041004 (2013).
[7] D. Vernardou, M. E. Pemble, and D. W. Sheel, Chem. Vap. Depos. **13**, 158–162 (2007).
[8] C. Piccirillo, R. Binions, and I.P. Parkin, Chem. Vap. Depos. **13**, 145–151 (2007).
[9] T. Manning, I. Parkin, C. Blackman, and U. Qureshi, J. Mater. Chem. **15**, 4560–4566 (2005).
[10] A. Gentle, A. Maaroof, and G. Smith, Nanotechnology **18**, 025202 (2007).
[11] N. Bahlawane and D. Lenoble, Chem. Vap. Depos. **20**, 299–311 (2014).
[12] K. Martens, N. Aetukuri, J. Jeong, M. G. Samant, and S.S. Parkin, Appl. Phys. Lett. **104**(8), 081918 (2014).
[13] J. B. Kana, J. M. Ndjaka, G. Vignaud, A. Gibaud, and M. Maaza, Opt. Commun. **284**(3), 807–812 (2011).
[14] M. Field and I. Parkin, J. Mater. Chem. **10**, 1863–1866 (2000).
[15] T. Manning and I. Parkin, J. Mater. Chem. **14**, 2554–2559 (2004).
[16] M. E. Warwick and R. Binions, J. Solid State Chem. **214**, 53–66 (2014).
[17] L. Crociani, G. Carta, M. Natali, V. Rigato, and G. Rossetto, Chem. Vap. Depos. **17**, 6–8 (2011).

[18] J. Livage, G. Guzman, F. Beteille, and P. Davidson, J. Sol-Gel Sci. Technol. **8**, 857–865 (1997).
[19] J. Livage, Solid State Ion. **86–88,** 935–942 (1996).
[20] I. Muylaert, J. Musschoot, K. Leus, J. Dendooven, C. Detavernier, and P. Van Der Voort, Eur. J. Inorg. Chem. **2012**, 251–260 (2012).
[21] J. Musschoot, D. Deduytsche, R. L. Van Meirhaeghe, and C. Detavernier, ECS Trans. **25**(4), 29–37 (2009).
[22] G. Rampelberg, K. Devloo-Casier, D. Deduytsche, M. Schaekers, N. Blasco, and C. Detavernier, Low temperature plasma-enhanced ALD of vanadium nitride as copper diffusion barrier, in: 13th Int. Conf. on Atomic Layer Deposition (ALD 2013).
[23] J. Y. Suh, R. Lopez, L. C. Feldman, and R. F. Haglund, Jr, J. Appl. Phys. **96**(2), 1209–1213 (2004).
[24] M. Miller and J. Wang, J. Appl. Phys. **117**, 034307 (2015).
[25] A. P. Peter, K. Martens, G. Rampelberg, M. Toeller, J. M. Ablett, J. Meersschaut, D. Cuypers, A. Franquet, C. Detavernier, J.-P. Rueff, M. Schaekers, S. Van Elshocht, M. Jurczak, C. Adelmann, and I. P. Radu, Adv. Funct. Mater. DOI 10.1002/adfm.201402687 (2014).
[26] L. Hongwei, L. Junpeng, Z. Minrui, T.S. Hai, S.C. Haur, Z. Xinhai, K. Lin, Opt. Express **22**, 30748–30755 (2014).
[27] X. J. Wang, H. D. Li, Y. J. Fei, X. Wang, Y. Y. Xiong, Y. X. Nie, and K. A. Feng, Appl. Surf. Sci. **177**(1), 8–14 (2001).
[28] C. Wen, L. Mai, J. Peng, Q. Xu, and Q. Zhu, J. Solid State Chem. **177**(1), 377–379 (2004).
[29] V. S. Vikhnin, I. N. Goncharuk, V. Y. Davydov, F. A. Chudnovskii, and E. B. Shadrin, Phys. Solid State **37**, 1971–1978 (1995).
[30] R. G. Mani and S. Ramanathan, Appl. Phys. Lett. **91**, 062104 (2007).
[31] P. Schilbe, Physica B **316**, 600–602 (2002).
[32] T.-H. Yang, J. Mater. Res. **25**(3), 422–426 (2010).
[33] T. D. Manning and I. P. Parkin, Polyhedron **23**(18), 3087–3095 (2004).
[34] N. Nandakumar and E. Seebauer, Thin Solid Films **519**, 3663–3668 (2011).